Leveraging Corkscrew Patrol Orbits to Improve Custody of Closely Spaced Objects

Erin Griggs, Sydney Bonbrest, Matt Schierholtz, Mark Bolden, Islam Hussein, Tom Kubancik
Trusted Space, Inc.

Blair Thompson
United States Air Force Academy

ABSTRACT

Patrol orbits were introduced in Ref. [1] as a family of orbits in the neighborhood of a geosynchronous equatorial orbit (GEO) created by introducing eccentricity to typical geosynchronous orbits. In this paper, we demonstrate the utility of satellites in patrol orbits to a deterrence architecture for assets in GEO. A proliferated constellation of low-cost satellites in patrol orbits can add immense value to existing and upcoming GEO missions by accumulating fundamental knowledge of the state of the GEO environment and acting as a neighborhood watch function, especially when ground sites are unable to observe or support. The satellites in patrol orbits provide additional geometric diversity to the observable state of GEO assets, and, if used for orbit determination (OD), can reduce uncertainty for closely spaced objects in the GEO belt.

This paper aims to build upon the previous patrol orbit work to present an updated and simplified algorithmic formulation of an asynchronous type of patrol orbit. Additionally, this paper develops a conceptual use case for a constellation of satellites in patrol orbits around a specific set of GEO assets. This constellation of patrol satellites provides deterrence through surveillance, providing space domain awareness of the region surrounding the GEO belt as a "neighborhood watch" function. With the proposed patrol orbits, we demonstrate OD of the GEO assets through electro-optical observations.

1. INTRODUCTION AND PREVIOUS WORK

Assets in geosynchronous equatorial orbits (GEO) are of high importance and utility, as they provide communications, broadcast, Earth-observation, and navigation services to military, academic, and civilian users. Their particular altitude of 35,786 km above the Earth's equator results in an orbital period equal to that of the rotation rate of the Earth, enabling the satellite to have a (nearly) fixed position in the sky with respect to a ground observer. Operators of GEO satellites must have knowledge of the satellite's surrounding environment, as it is continually becoming more contested. In his testimony to the Senate Armed Services Committee's strategic forces subcommittee in March 2023, the U.S. Space Force chief of operations, General B. Chance Saltzman, described China's latest capability to control and move satellites. He warned that China is "likely pursuing anti-satellite systems able to destroy satellites in geosynchronous orbit" [2]. Coverage of and around these high-valued GEO assets is imperative to deter any potential nefarious actions.

Satellites in patrol orbits adjacent to the GEO belt could provide monitoring, observation, and support that is complementary to services traditionally provided by the ground. Patrol orbits were introduced in Ref. [1] as a family of orbits in the neighborhood of a GEO, created by introducing eccentricity to a typical geosynchronous orbit. A follow-on study described different strategies and concepts of operations (CONOPS) to use patrol orbits for space domain awareness (SDA) [3]. This paper will focus on three novel areas of research: (1) the formulation and simplified

Copyright © 2024 Advanced Maui Optical and Space Surveillance Technologies Conference (AMOS) – www.amostech.com

mathematical description of a new asynchronous corkscrew patrol orbit type, (2) the investigation and optimization of an architecture of satellites in patrol orbits for surveillance of a specific region of the GEO belt, and (3) the enhanced orbit determination (OD) and cataloging of GEO assets through a combination of simulated ground- and space-based electro-optical (EO) observations.

This paper introduces a new type of patrol orbit that we describe as the "asynchronous corkscrew". We provide a description of the algorithm formulation of this patrol orbit type, which includes a notable improvement to the complexity of the mathematical derivation and process. The flight profile of the corkscrew orbit is explored, including longitudinal and zonal coverage, retro- and pro-grade configurations, and a description of motion over time through the orbit lifecycle. We compare this patrol orbit to previous patrol orbit types described in Ref. [1] and Ref. [3], in terms of surveillance capability and orbit maintainability. We also investigate the delta-V requirements to move between corkscrew orbits and previously-investigated patrol orbits.

We then explore the utility of satellites in patrol orbits for the surveillance and tracking of objects in a particular region of the GEO belt. This investigation will focus on patrolling a region around the pair of Anik satellites, co-located in the GEO belt at 107.3°W longitude. These Canadian telecommunications satellites, Anik F1 and Anik F1R, are challenging to distinguish separately by ground-based EO means because of a separation of 0.03° in longitudinal position [4, 5]. We develop an architecture of patrol satellites equipped with an EO payload to observe a specified region about the Anik satellites. Using a subset of the optical sensor pointing strategies described in Ref. [3], we conduct trades of patrol satellite constellation characteristics, including categories of patrol orbits, configuration, flight profile dynamics, and total number of satellites participating in the surveillance activities. We aim to optimize longitudinal/zonal coverage, revisit times, and custody of the Anik satellites.

Finally, we investigate the OD of the Anik satellites via a combination of EO observations from the proposed patrol orbits and from the ground. Through modeling and simulation (M&S), we generate optical observations to be received by ground-based EO observers and the optical payloads onboard the patrol satellites and characterize their uncertainties. These observations are processed by a two-body OD filter to estimate the position and velocity of the Anik satellites. We compare the accuracy and uncertainty of a ground-based solution versus one where we use patrol satellite observations, with the goal to show improvement to the OD accuracy and uncertainty estimates using a spatially diverse set of space-based observers. We also aim to demonstrate the robustness of the multi-observer patrol satellite constellation to cross-tagging by the closely-spaced Anik satellites, and to ground station outages.

2. GEOSYNCHRONOUS PATROL ORBIT

2.1. Overview

The nominal geosynchronous orbit is circular and equatorial. The resulting orbit and ground tracks are single, stationary points in Earth-fixed coordinates. If the GEO orbit has some non-zero inclination, the orbit and ground tracks will appear to be north-south "figure-eight" shaped in Earth-fixed coordinates. The maximum (and minimum) latitude will be equal to the inclination angle, i. If the GEO orbit has some non-zero eccentricity, e, the inertial velocity will vary between some minimum and maximum values as the satellite moves between apogee and perigee, respectively. There will also be altitude variations between apogee and perigee. The result in Earth-fixed coordinates is east-west and radial (i.e., altitude) motion over a period of one GEO orbit (≈ 24 hours). When combined with non-zero inclination, the resulting Earth-fixed orbit track is a quasi-elliptical closed path – a *patrol orbit* [1]. A spacecraft with this orbit will be moving around (i.e., "patrolling") a region of the GEO belt – the *patrol zone*. Inclination and eccentricity are independent parameters and can be chosen to optimize mission objectives. An example patrol orbit is shown in Figure 1.

A patrol orbit improves viewing geometry for observing GEO resident space objects (RSOs) [1, 3]. A patrol orbit might also be considered for loitering in a "holding pattern" of on-orbit GEO servicing and repair spacecraft. Although similar to relative motion between two orbiting spacecraft, there are distinct differences between patrol orbits and spacecraft relative motion. The patrol orbit is designed around the rotating Earth, independent from any spacecraft orbital dynamics. As such, the patrol orbit track is not restricted by the assumptions or constraints typical of spacecraft relative motion. The *longitude width*, $\Delta\lambda$, in degrees, of the patrol orbit is an input parameter that specifies the approximate east and west longitude boundaries around the center longitude λ_c in degrees.

Copyright © 2024 Advanced Maui Optical and Space Surveillance Technologies Conference (AMOS) – www.amostech.com

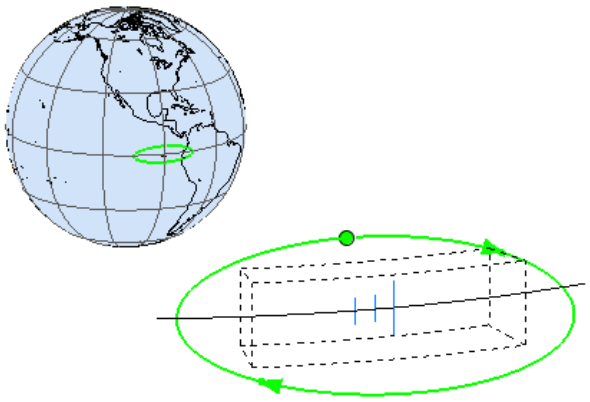

Fig. 1: Example patrol orbit (green) and patrol zone (dashed lines). At this scale, the figure-eight tracks of other objects in the patrol zone appear as thin vertical lines (blue).

The orientation of the patrol orbit quasi-plane within the longitude bounds is determined by the argument of perigee, ω of the patrol orbit. With $\omega = 90°$, the patrol orbit east-west axis is generally aligned with the GEO belt, resulting in a *lateral* patrol orbit (e.g., Figure 1). Argument of perigee $\omega = 0°$ or $\omega = 180°$ results in a patrol orbit quasi-plane that is more perpendicular to the Earth's surface – a *vertical* patrol orbit (not shown here). The eccentricity required for a lateral patrol orbit ($\omega = 90°$) with longitude width $\Delta\lambda$ in degrees can be approximated by

$$e \approx \frac{\Delta\lambda}{218.537} - 0.00582 \tag{1}$$

2.2. Asynchronous Corkscrew Patrol Orbit

The entire patrol orbit can be made to drift east or west in Earth-fixed coordinates by altering the semi-major axis. Such asynchronous orbits are advantageous for repositioning patrol orbit spacecraft without changing the Earth-fixed orbit track shape. Decreasing semi-major axis results in an eastward drift, while increasing the semi-major axis results in a westward drift.

The semi-major axis, a, needed for a drift rate of $\dot{\lambda}$ (deg/day) can be computed using Eq. (2),

$$a = \left[\mu \left(\omega_{\oplus} + \frac{\pi \cdot \dot{\lambda}}{15\,552\,000} \right)^{-2} \right]^{1/3} \quad \text{meters} \tag{2}$$

with constants

$$\mu = 3.986\,004\,415 \times 10^{14} \quad \mathrm{m^3/s^2}$$
$$\omega_{\oplus} = 7.292\,115 \times 10^{-5} \quad \mathrm{rad/s}$$

The sign of $\dot{\lambda}$ determines the drift direction – positive for eastward drift, negative for westward.

With the proper combination of inclination, eccentricity, and semi-major axis, an asynchronous *corkscrew* patrol orbit can be established that drifts either east or west around the GEO belt. This type of orbit could be very useful for proximity surveillance along the entire GEO belt while maintaining observation viewing diversity. The re-visit rate for the entire GEO belt is determined by the longitude drift rate, $\dot{\lambda}$in degrees/day.

Copyright © 2024 Advanced Maui Optical and Space Surveillance Technologies Conference (AMOS) – www.amostech.com

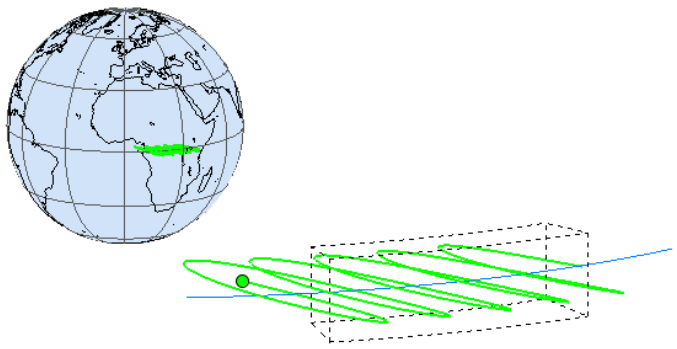

Fig. 2: Example of a corkscrew patrol orbit.

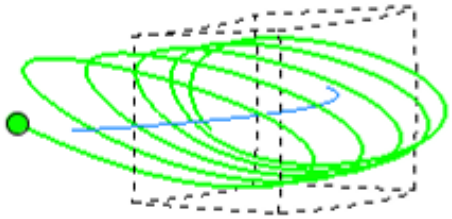

Fig. 3: Example of a corkscrew patrol orbit – alternate view.

An example asynchronous corkscrew patrol orbit is shown in Figures 2 and 3. In this example, the corkscrew patrol orbit parameters are:

$$\begin{aligned} \Delta\lambda &= 8 \quad \text{deg} \\ \dot{\lambda} &= 2 \quad \text{deg/day} \\ i &= 2 \quad \text{deg} \\ \omega &= 180 \quad \text{deg} \\ a &= 42\,009\,151.207 \quad \text{meters} \\ e &= 0.030\,753 \end{aligned}$$

The longitude drift rate of $\dot{\lambda} = 2$ deg/day enables progressive surveillance of the entire GEO belt every ≈ 180 days.

2.3. Asynchronous Drift Orbit Characterization

An orbit is considered asynchronous when $\dot{\lambda} \neq 0^\circ$ per day. Vertical and lateral patrol orbits have $\dot{\lambda} = 0^\circ$, while corkscrew patrol orbits are asynchronous. When the longitude drift rate has a higher $\dot{\lambda}$, the patrol satellite has a smaller period around the Earth. The impact of a $\dot{\lambda}$difference is demonstrated in the Earth-fixed frame in Figure 4.

Copyright © 2024 Advanced Maui Optical and Space Surveillance Technologies Conference (AMOS) – www.amostech.com

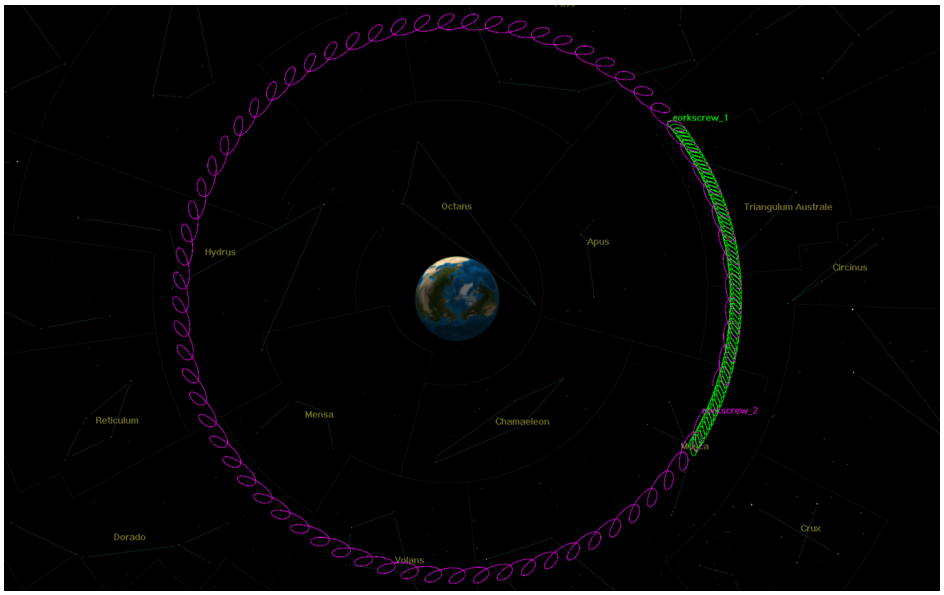

Fig. 4: Two asynchronous corkscrew patrol orbits propagated over 70 days, one with $\dot{\lambda} = 5°$ (green) and the other with $\dot{\lambda} = 8°$ (purple).

Patrol orbits of types lateral, vertical, and asynchronous corkscrew are plotted together in the Earth-fixed frame in Figure 5. This figure demonstrates the different characteristics corkscrew orbits have when compared to lateral and vertical patrol orbits. While corkscrew orbits span the entire GEO belt, lateral and vertical continuously patrol the same local area of the GEO belt.

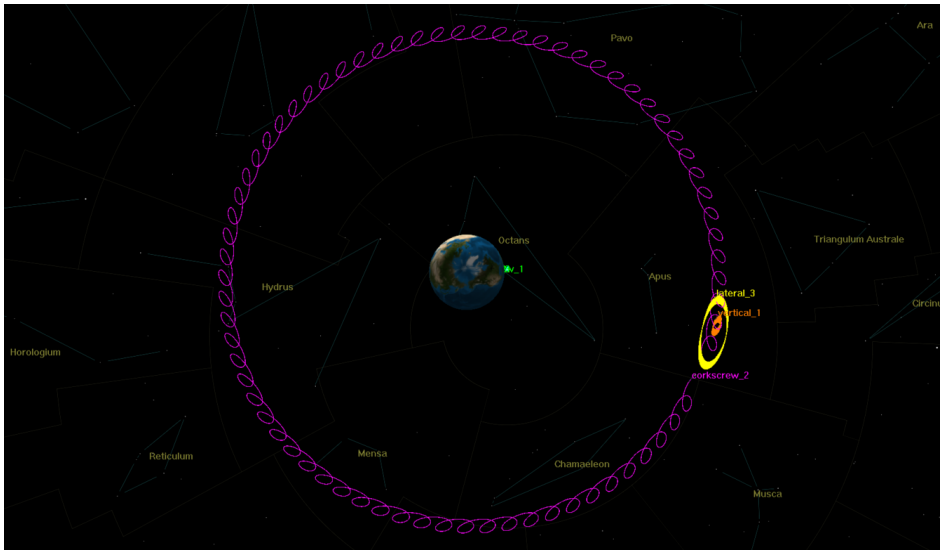

Fig. 5: The three different patrol orbits propagated over 70 days. The asynchronous corkscrew orbit is shown in purple, the lateral orbit in yellow, and the vertical orbit in orange.

As described in Section 2, we distinguish the lateral and vertical patrol orbits mathematically by their argument of perigee, ω. This difference can be better understood through a ground-based perspective, as shown in Figure 6. The lateral orbit appears to be parallel to the Earth's equatorial plane while the vertical orbit appears perpendicular. This is achieved through variation of their argument of perigee: lateral orbits can have an ω of 90° or 270° while vertical orbits can either be 0° or 180°.

Copyright © 2024 Advanced Maui Optical and Space Surveillance Technologies Conference (AMOS) – www.amostech.com

Fig. 6: An example vertical (green) and lateral (blue) patrol orbit as viewed from a projection map of the Earth's surface.

To understand the stability of each of the patrol satellites over time, we propagated examples from the three patrol orbit types for three years and examined their Keplerian elements. Semi-major axis, eccentricity, and inclination for each patrol orbit is plotted over time and shown in Figure 7. The orbits show consistency in semi-major axis and eccentricity, and some drift in inclination. Although the orbits are fairly stable, mission designers and operators should keep a supply of fuel available as a resource for future orbital maintenance maneuvers, especially to counter inclination drift. A baseline delta-V budget for any type of patrol orbit for a 5-year mission can be found in Ref. [1].

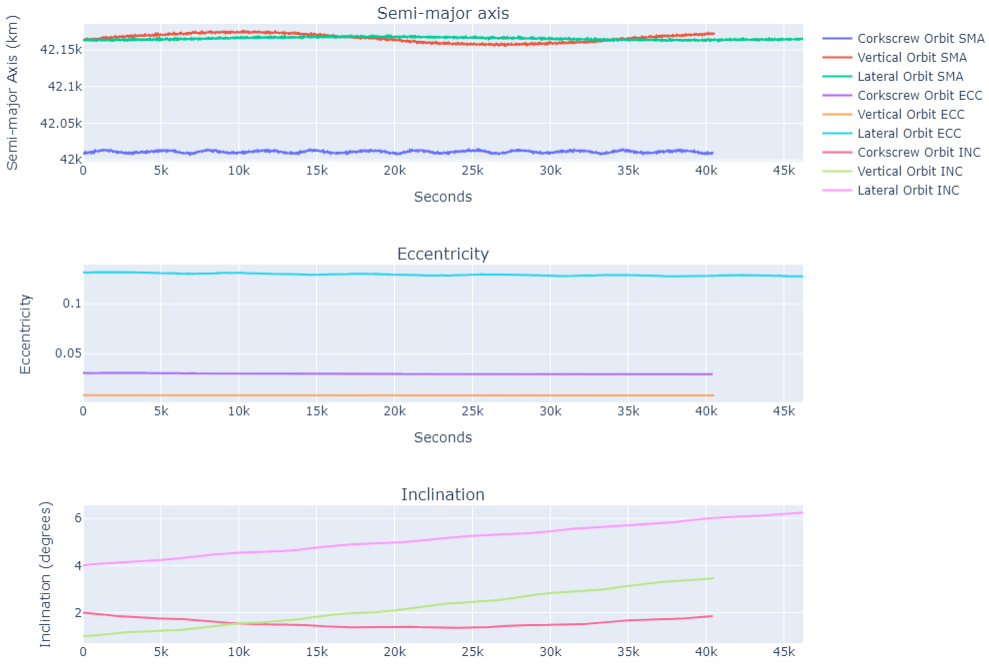

Fig. 7: Semi-major axis, eccentricity, and inclination for all three patrol orbits types propagated for three years.

Copyright © 2024 Advanced Maui Optical and Space Surveillance Technologies Conference (AMOS) – www.amostech.com

3. INVESTIGATION OF REGIONAL UTILITY OF PATROL ORBITS

3.1. Design Reference Mission

Satellites in patrol orbits have the potential to provide enhanced surveillance ability due to better lighting and range conditions. In this paper, we explore an illustrative scenario where we model satellites in the various patrol orbit categories described above to monitor a region of the GEO belt. We focus on the observation of a pair of Canadian telecommunications satellites, Anik F1 and Anik F1R, whose close proximity in the GEO belt is a subject of multiple studies [6, 7, 8].

Anik F1 and F1R are co-located in the geostationary belt of satellites at approximately 107.3°W longitude. Conclusively distinguishing these two satellites by ground-based optical methods of orbit determination prove to be challenging, as angular errors compound at a rate of 200 meters of position error for each arcsecond of angular error [9]. For example, an optical ground station with 0.01° of antenna pointing error results in greater than 7 km of position error at geostationary distances. Additionally, ground-based methods are subject to lighting constraints, allowing for object surveillance at limited times throughout the day.

We aim to circumvent these challenges through observation of the Anik pair of satellites by satellites with realistic optical payloads in nearby patrol orbits. In the next section, we conduct analyses to optimize the number of detections of the Anik satellites by varying the formulation of three patrol orbit types: lateral, vertical, and asynchronous corkscrew. Using these patrol satellites with orbital characteristics that optimize monitoring the Anik satellites, we conduct an OD assessment and compare to ground-based OD.

3.2. Optimization of Observer Constellation

To understand how well the satellites in patrol orbits detect one of the targets, we used our end-to-end Modeling & Simulation (M&S) environment that combines high-fidelity orbit modeling, using General Mission Analysis Tool (GMAT) with a Python-based signal-to-noise ratio (SNR) analysis tools. These M&S capabilities allowed us to optimize characteristics of the patrol orbit in order to maximize the number of "detections" between the observer and a target satellite. In this case, the observer is a given patrol satellite and the targets are Anik F1 and F1R.

In these simulations, detections are defined as an instance where the SNR of the observation is above a minimum value. Here we use an SNR of 6. The observation SNR values are based on a variety of aspects including geometry, line of sight from the patrol satellite to the observed satellite, satellite orientation, and lighting conditions. Our M&S environment also has the ability to model different pointing strategies, optical payloads, and detector packages for the observing spacecraft. On-board the observer satellites in patrol orbits, we modeled a realistic optical payload and detector package. The detector package model has a resolution of 2,048 x 2,048 pixels and a quantum efficiency of 85 %. Our optics payload model has a focal length of 0.9 meters, an aperture diameter of 0.45 meters and an effective aperture diameter of 0.42 meters.

Two pointing strategies were leveraged to optimize the observer constellation: off-nadir and targeted pointing. Off-nadir is a pointing strategy where the sensor points at a fixed offset from nadir. It takes lighting conditions into account to decide whether to look forward or backward in velocity direction. As described in Ref. [3], the off-nadir pointing strategy outperformed two other investigated pointing strategies: 4π scanning (a scan of a Fibonacci sphere of points) and solar opposition (sensor fixed to the sun vector). In targeted pointing, the observer satellite directly points its sensors at a specific target of interest, in this case, the Anik F1 and F1R satellites. During this constellation optimization phase, we assume knowledge of the Anik satellites' ephemerides; therefore, the targeted pointing method is a valid method to optimize detection.

To determine which pointing strategy was the best one to utilize, a comparison analysis was done between the two. This analysis showed that the off-nadir strategy performs better than the direct targeting strategy. Detections from a lateral patrol orbit observing Anik F1 for one month using both pointing methods is shown in Figure 8. The off-nadir method outperforms the targeted method and is a more realistic pointing strategy for an unknown target. While the targeted method is a valid choice to use for this case, it uses assumed knowledge of the Anik satellite's ephemerides, which could differ from the truth.

After refining the models for simulated instruments and pointing strategies, we then fine-tuned the patrol orbits themselves. The key to optimizing each patrol orbit is to know which orbital element is the most logical to adjust, as there

Copyright © 2024 Advanced Maui Optical and Space Surveillance Technologies Conference (AMOS) – www.amostech.com

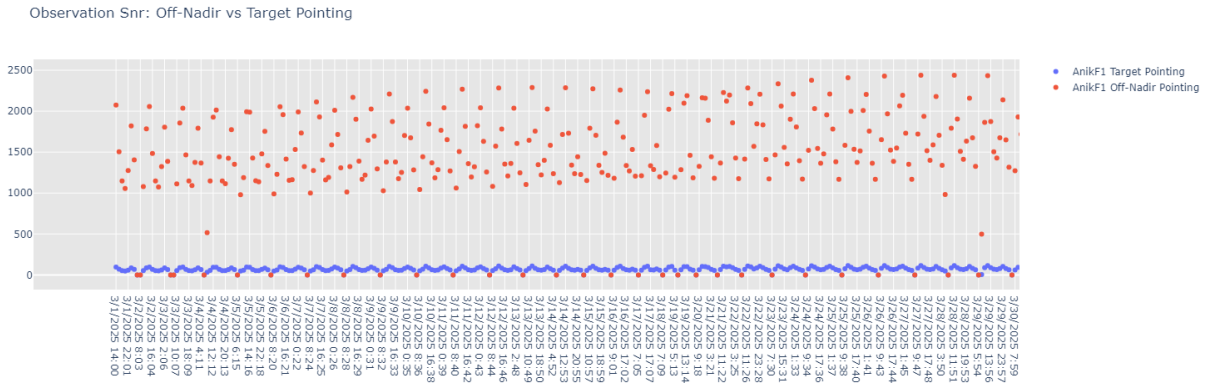

Fig. 8: Comparison of two pointing strategies for an observer satellite in a lateral patrol orbit.

are limitations in terms of what can or cannot be altered. A nominal "Configuration 1" was created for satellites in vertical, lateral, and asynchronous corkscrew patrol orbits, the corresponding values are shown in Table 1.

Table 1: Configuration 1 definition for the three patrol orbit types.

Satellite	a (km)	e (unitless)	i (°)	Ω (°)	ω (°)	ν (°)
Lateral	42164.173	0.0436	2	324.546	270	0
Vertical	42164.172	0.00873	2	236.0456	0	0
Corkscrew	42009.151	0.0308	2	44.545	180	0

3.2.1. Lateral Patrol Orbit Variation

In an attempt to maximize detections, longitude width ($\Delta\lambda$) was varied for a series of lateral patrol orbits. Longitude width directly affects eccentricity of the patrol satellite which will increase or decrease its maximum distance away from the target. Upon analysis, a longitude width of 5° maximized detection results. Figure 9 shows a comparison of the number of detections found over one month using three different lateral patrol orbits with different longitude width variations, with "Configuration 1" defined as in Table 1. The simulation represented by Figure 9 is a satellite in a lateral orbit observing Anik F1 with an off-nadir pointing strategy.

Fig. 9: Comparison of number of detections by three different lateral patrol orbit configurations over one month. Configuration 1 has $\Delta\lambda = 10°$, Configuration 2 $\Delta\lambda = 5°$ and Configuration 3 has $\Delta\lambda = 1°$.

Copyright © 2024 Advanced Maui Optical and Space Surveillance Technologies Conference (AMOS) – www.amostech.com

3.2.2. Vertical Patrol Orbit Variation

Similar to lateral patrol orbits, a variation of different longitude widths were explored in an attempt to maximize the number of vertical patrol orbit detections of the Anik satellites. Analysis of different longitude width variations showed a $\Delta\lambda = 3°$ maximized the Anik satellite detections. Figure 10 shows the results of two different configurations of vertical patrol orbits with an off-nadir pointing strategy while observing Anik F1. Configuration 1 has the same values shown previously in Table 1.

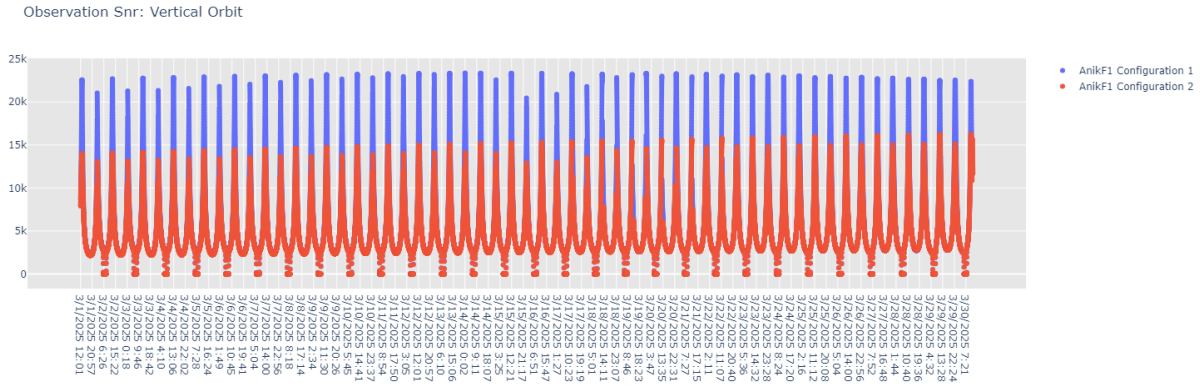

Fig. 10: Comparison of number of detections by two vertical patrol orbits over one month. Configuration 1 has $\Delta\lambda = 3°$ and Configuration 2 has $\Delta\lambda = 5°$

.

3.2.3. Corkscrew Patrol Orbit Variation

The longitude drift rate was varied during the investigation of asynchronous corkscrew orbits in an attempt to understand whether detection can be maximized with a slow corkscrew orbit that spends more continuous time over a target, or a faster corkscrew orbit that passes non-continuously over the target more often. When comparing detections for Anik F1 vs Anik F1R, there was more detection observed for the configuration with the smaller longitude drift rate. Figure 11 displays the detections recorded for two different corkscrew configurations that are observing Anik F1 with an off-nadir pointing strategy.

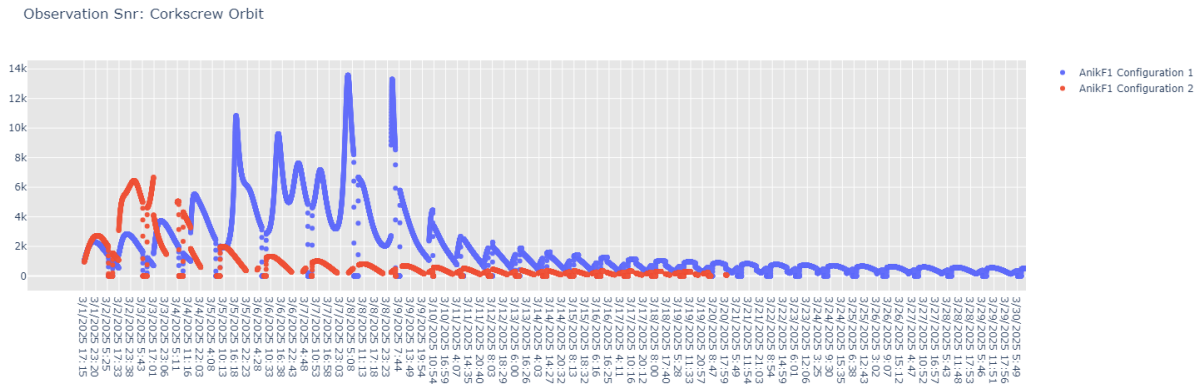

Fig. 11: Comparison of number of detections by two corkscrew orbits over one month. Configuration 1 has $\dot{\lambda} = 2°$ per day and Configuration 2 has $\dot{\lambda} = 6°$ per day

.

Copyright © 2024 Advanced Maui Optical and Space Surveillance Technologies Conference (AMOS) – www.amostech.com

3.2.4. Patrol Orbit Optimization Conclusions

These trade studies yielded the following conclusions:

- In the short term (studies of less than 30 days), surveillance from asynchronous corkscrew patrol orbits benefit from smaller longitudinal drift rates, as they will spend more time over their desired target.
- Lateral and vertical patrol orbits need a "Goldilocks" longitudinal width, as to not be too close or to far from the target to optimize detections.
- Lateral and vertical patrol orbits provide concentrated viewing of a particular region of the GEO belt.
- Asynchronous corkscrew orbits are useful for slow monitoring of the entire GEO belt, but more investigation is needed to determine if a slow longitudinal drift rate outweighs a higher drift rate with more revisit opportunities.

3.3. Orbit Determination Study

In the final phase of this study, we applied our optimized orbit characteristics for each category of patrol orbit and assessed their ability to conduct orbit determination of the pair of Anik satellites. Using EO observations generated by our M&S environment, we estimate the position and velocity states of the Anik satellites over two periods of time: four hours and for a full day. Through these simulations, we assess and compare the OD estimation results for an RSO from each patrol orbit type, and by a fictitious single, ground-based observer with unobstructed visibility to the Anik satellites in Colorado Springs, Colorado.

Initial Conditions

The initial conditions for the Anik satellites and ground station observer are shown in the tables below.

Epoch: August 14, 2024, 00:00:00.000 UTC

Table 2: Initial states for the Anik F1 and F1R satellites at the epoch (in J2000).

Satellite	a (km)	e (unitless)	i (°)	Ω (°)	ω (°)	ν (°)
Anik F1	42165.633	9.450 e-4	3.600	83.118	49.088	81.293
Anik F1R	42165.666	3.620e-4	2.730	85.038	43.053	87.241

Table 3: Ground station location (in geodetic latitude, longitude, and altitude).

Ground Station	Latitude (°)	Longitude (°)	Altitude (km)
Colorado Springs	38.87	255.08	1.8

Observation satellites were placed in patrol orbits with the following characteristics.

Table 4: Initial patrol orbit characteristics for Anik orbit determination study (in J2000).

	λ_c (°)	$\Delta\lambda$ (°)	$\dot{\lambda}$ (°/day)	i (°)	ω (°)	ν_0 (°)
Lateral	-108.5	5.0	0.0	1.0	90.0	0.0
Vertical	-108.5	2.0	0.0	1.0	0.0	0.0
Corkscrew	-109.5	8.0	2.0	2.0	180.0	0.0

Using the algorithms described in Section 2, we translate these patrol orbit characteristics into Keplerian orbital elements that describe the state of the patrol satellite at the initial epoch.

Measurement Generation

The Runge-Kutta-Fehlberg 7(8) (RKF78) numerical integration method is employed to compute the *truth* states during propagation using the Pines' formulation of the Earth's gravity model [10, 11]. For the *truth* states, we use a high-fidelity gravity model of degree and order 10. The true observer and RSO position and velocity values are simulated

Copyright © 2024 Advanced Maui Optical and Space Surveillance Technologies Conference (AMOS) – www.amostech.com

at the desired cadence over the simulation period: for the four-hour simulation, the cadence is 60 seconds, and for the full-day simulation, the cadence is 300 seconds. The *truth* Right Ascension (RA) and Declination (DEC) values are calculated between observer and RSO in a J2000 reference frame. We assume the patrol satellites are equipped with Global Navigation Satellite System (GNSS) receivers adapted for operation at geostationary altitude, while we estimate the states of the RSO using RA and DEC observations made from the patrol satellite [12, 13].

Measurement noise is added to the *truth* optical observations (RA and DEC) and to the observer's position and velocity state, as the patrol satellite is not a stationary observer and also has uncertainty in its state. For the purposes of this academic study, the following assumptions are made for the generation of simulated noise to be added to the measurements: 1) the satellites in patrol orbits carry an M-code GNSS receiver, similar in capability to the Sentinel receiver described in Ref. [12], with self-orbit knowledge of 25 meters 1-σ in position, and 2 cm/s 1-σ in velocity at geostationary altitudes; and 2) the optical payloads on the patrol satellites are similar to those described in Ref. [9], and are able to discern angular measurements (RA and DEC) with 1-σ of 4 arcseconds.

To enhance the fidelity of the simulation, we applied a filter to the generated observations that allowed only those that are physically possible by a realistic detector and optical payload onboard the spacecraft. This filter was applied to the set of observations generated for 24 hours. First, lighting and solar phase angle constraints were applied to reduce the number of valid observations. The observations were filtered to only allow observations above an SNR of 6, assuming the onboard optical payload and detector described in Section 3.2. Finally, the off-nadir pointing strategy was employed because it was shown to produce the highest numbers of detections in comparison to other pointing strategies in Ref. [3]. Exercising these constraints on the observation generation resulted in (expected) detection gaps in the generated observations.

RA and DEC optical observations were also simulated from a ground station observer. The relative states between the ground observer at Colorado Springs, Colorado to the Anik satellites were calculated at 300 second intervals for 24 hours. We assumed perfect knowledge of the ground station position and assumed measurement noise of 1 arcsecond in RA and DEC [9]. The observations were filtered by a daylight constraint, allowing for valid measurements only during umbra and penumbra.

Summary tables of measurement generation process and added measurement noise are given in Tables 5 and 6.

Table 5: Summary of measurement generation for simulated orbit determination study scenarios.

Simulation Length	Observation Cadence	Observer Types	Measurements
4 hours	60 sec	Patrol orbits only	All
24 hours	300 sec	Patrol orbits + ground station	Filtered for physical constraints

Table 6: Summary of the simulated measurement noise.

Space-based Observations	RA DEC	Mean = 0 arcsec StdDev = 4 arcsec
Patrol Orbit State Errors (GNSS-based)	Position Velocity	Mean = 0 m StdDev = 25 m Mean = 0 m/s StdDev = 0.02 m/s
Ground-based Observations	RA DEC	Mean = 0 arcsec StdDev = 1 arcsec

Orbit Determination Filters

For the patrol satellite to Anik orbit determination cases, a two-body, 12-state Extended Kalman Filter (EKF) that estimates both observer (patrol satellite) and RSO (Anik satellite) states was implemented. As there is uncertainty in both the observer and RSO states at any given point in time, we use this combined EKF to concurrently estimate the position and velocity states of both satellites with each observation. The authors make note that the EKF was

Copyright © 2024 Advanced Maui Optical and Space Surveillance Technologies Conference (AMOS) – www.amostech.com

not overly tuned in this work, as the purpose of the study is to see the general effects of using satellite-based optical measurements for orbit determination of GEO objects. Additional filter tuning and optimization is recommended for follow-on studies and experiments.

A total of 12 OD analyses with the EKF were performed: for each of the patrol orbit types (lateral, vertical, and corkscrew) to each of the Anik satellites (F1 and F1R) for 4 hours (all observations) and for 24 hours (filtered observations). The *a priori* state estimate, x_0, for each of these runs was initialized to the truth state of the respective Anik satellite; however, for the 24-hour simulations, errors sampled from continuous uniform distributions were added to each component of the position and velocity states as follows: $\mathcal{U}$(-50,50) m in x, y, z and $\mathcal{U}$(-0.05,0.05) m/s in v_x, v_y, v_z. The diagonal elements of the *a priori* covariance matrix, P_0, corresponding to the initial state of the patrol satellite were initialized to 50 m^2 in position and 2 cm^2 in velocity. The diagonal elements of P_0 corresponding to the initial state of the RSO were initialized to 200 m^2 in position and 2 cm^2 in velocity. The diagonal elements of the measurement error variance, R, were initialized to 50 m^2 for the GNSS measurement noise and 10 arcsec for RA and DEC measurement noise. No process noise, Q, was modeled in this study. Similar to the observation generation process, the orbit propagation step employed the RKF78 numerical integrator, but with a reduced gravity model of degree and order 3.

For the ground-to-space orbit determination case, we used a 6-state Unscented Kalman Filter (UKF) to estimate the position and velocity states of the Anik satellites using optical RA and DEC measurements from a fixed ground site. The UKF uses a Dormand-Prince Runge-Kutta 8(5,3) integrator for propagation of the Anik satellites. The force models incorporated in the integrator include the Holmes-Featherstone Earth gravitational potential model, with order 72 and degree 72, and point masses for the Earth's moon, Jupiter and the sun. The RSO masses were modeled as 3015 kg. The initial states of the RSOs, P_0, were assumed to be well-known and no error was applied. The diagonal elements of the measured error covariance, R, were initialized to 1 arcsecond for RA and DEC. The diagonal elements of P, the propagated uncertainty, for the RSO were 10 m^2 in position and 5 mm^2/s^2 in velocity. The process noise Q was set to 10 m^2 in position and 1 mm^2/s^2 in velocity on the diagonal elements. Since the position and velocity of the ground station are assumed to be well known, no uncertainty in the sensor state was modeled for the 6-state UKF.

The filtering parameters are summarized in Table 7 for the 6-state UKF and Figure 8 for the 12-state EKF.

Table 7: Summary of filter noise values for the 6-state UKF.

			24-hour simulation
6-state UKF	x_0	x, y, z	x, y, z
		v_x, v_y, v_z	v_x, v_y, v_z
	P	x, y, z	10 m^2
		v_x, v_y, v_z	5 mm^2/s^2
	Q	x, y, z	10 m^2
		v_x, v_y, v_z	1 mm^2/s^2
	R	RA, DEC	1 arcsec

Table 8: Summary of filter noise values for the 12-state EKF.

			4-hour simulation	24-hour simulation
12 state EKF	x_0	x, y, z	x, y, z	x, y, z + U[-50, 50]m
		v_x, v_y, v_z	v_x, v_y, v_z	v_x, v_y, v_z + U[-0.05, 0.05]m/s
	P_0	x, y, z (observer)	50 m^2	
		v_x, v_y, v_z (observer)	2 cm^2/s^2	
		x, y, z (RSO)	200 m^2	
		v_x, v_y, v_z (RSO)	2 cm^2/s^2	
	R	x, y, z (GNSS)	50 m^2	
		RA, DEC	10 arcsec	

The 12-state filter outputs the errors in position and velocity relative to the *truth* orbits for the observer and RSO, as

Copyright © 2024 Advanced Maui Optical and Space Surveillance Technologies Conference (AMOS) – www.amostech.com

well as the measurement residuals for RA and DEC. The 6-state filter outputs errors in position and velocity relative to the *truth* orbits for each of the RSOs. In the following *Results* section, we show the OD filter outputs for the 4-hour simulation (with no observation filtering) as a first assessment and validation of filter performance. We then run the OD filters on the longer, 24-hour observation set, but process only the observations that were deemed detectable in our M&S environment, as described in the *Measurement Generation* section.

Results

A detailed subset of results are shown for the 4-hours of unfiltered observations made by the asynchronous corkscrew orbit while in close proximity to Anik F1 and F1R. Similar results for the vertical and lateral patrol orbits were found, however, for the sake of brevity, we show the detailed figures only for the corkscrew patrol orbit and summarize results for the other orbit types.

First, we demonstrate the OD errors in position and velocity for the patrol satellite itself using the uncertainties inherent in the GNSS measurements at GEO.

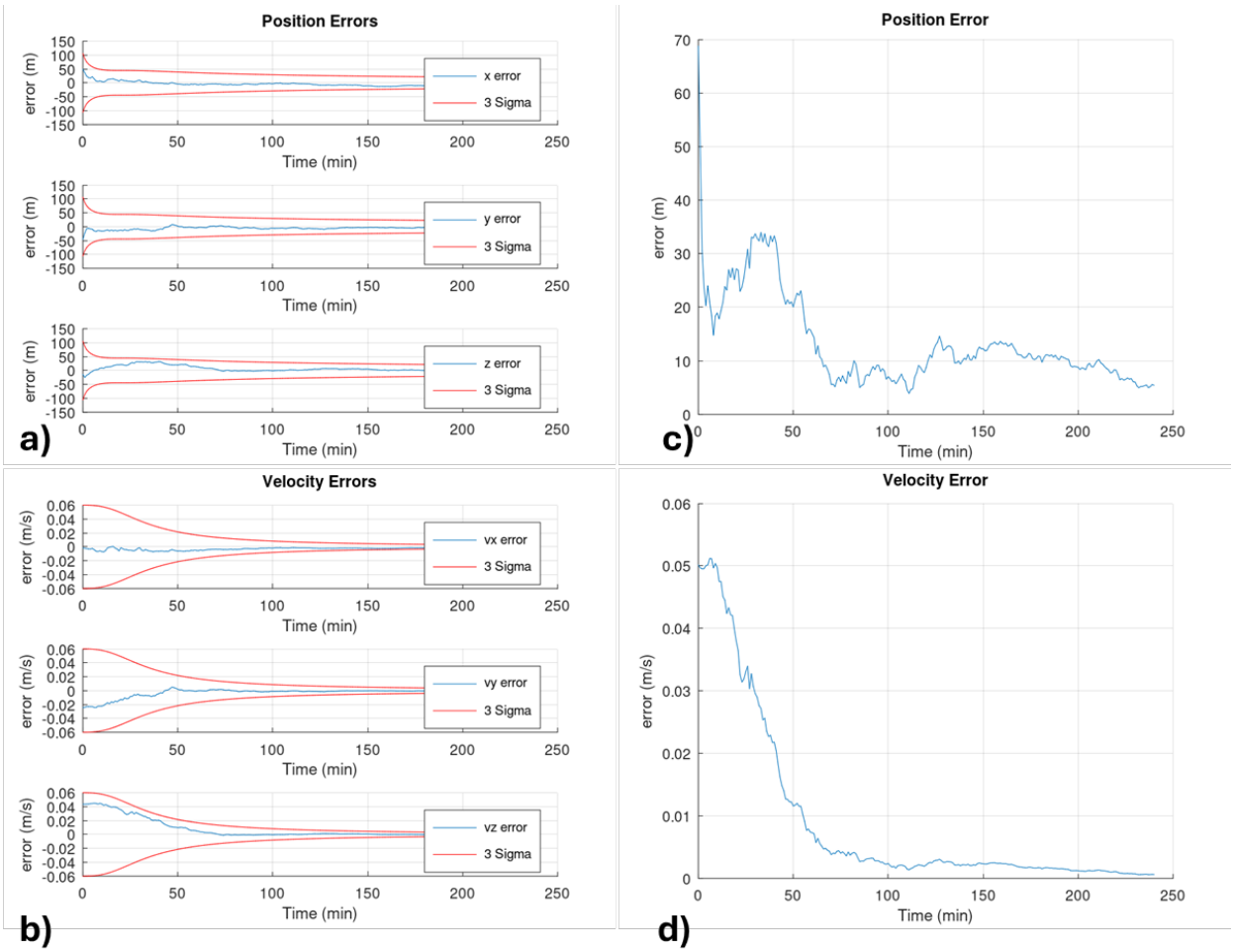

Fig. 12: Errors in position and velocity of the satellite in a corkscrew patrol orbit as solved by the EKF. Panels a) and b) show the position and velocity errors in each axis, along with the filter's 3-σ covariance bound. Panels c) and d) show the Euclidean norm of the component errors in position and velocity.

In Figures 13 and 14, the OD errors in position and velocity, and the RA and DEC measurement residuals are shown for each of the Anik satellites, respectively, as observed by the asynchronous corkscrew orbit.

Copyright © 2024 Advanced Maui Optical and Space Surveillance Technologies Conference (AMOS) – www.amostech.com

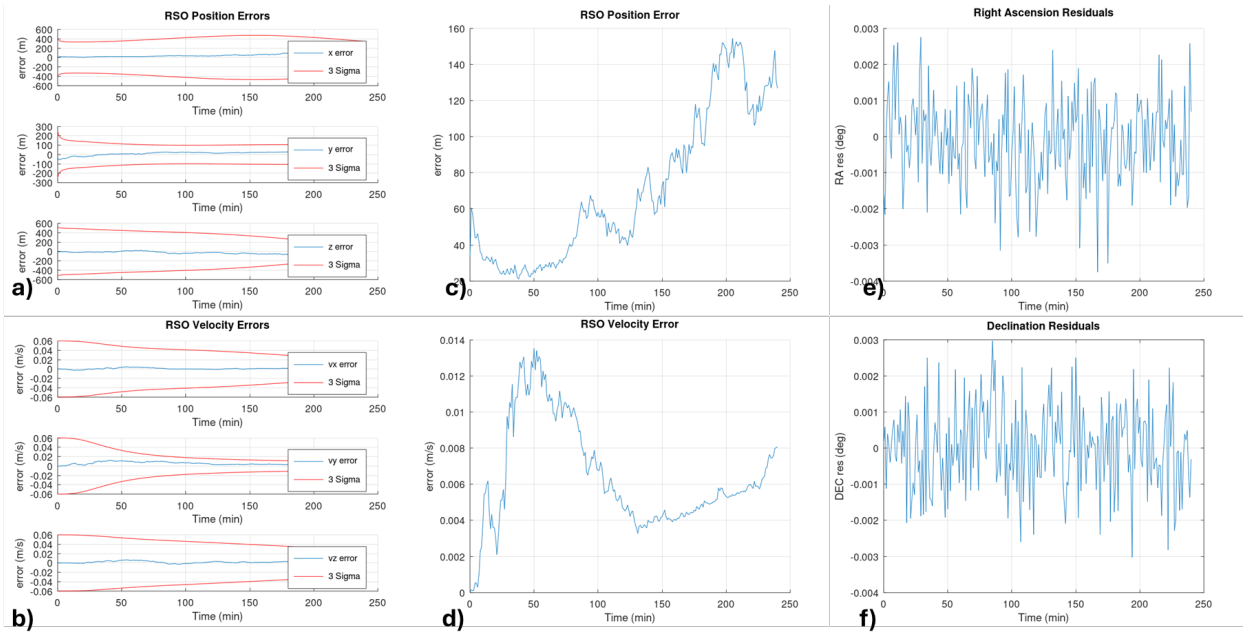

Fig. 13: Errors in position and velocity of Anik F1 as solved by the EKF. Panels a) and b) show the position and velocity errors in each axis, along with the filter's 3-σ covariance bound. Panels c) and d) show the Euclidean norm of the component errors in position and velocity. Panels e) and f) show the measurement residuals.

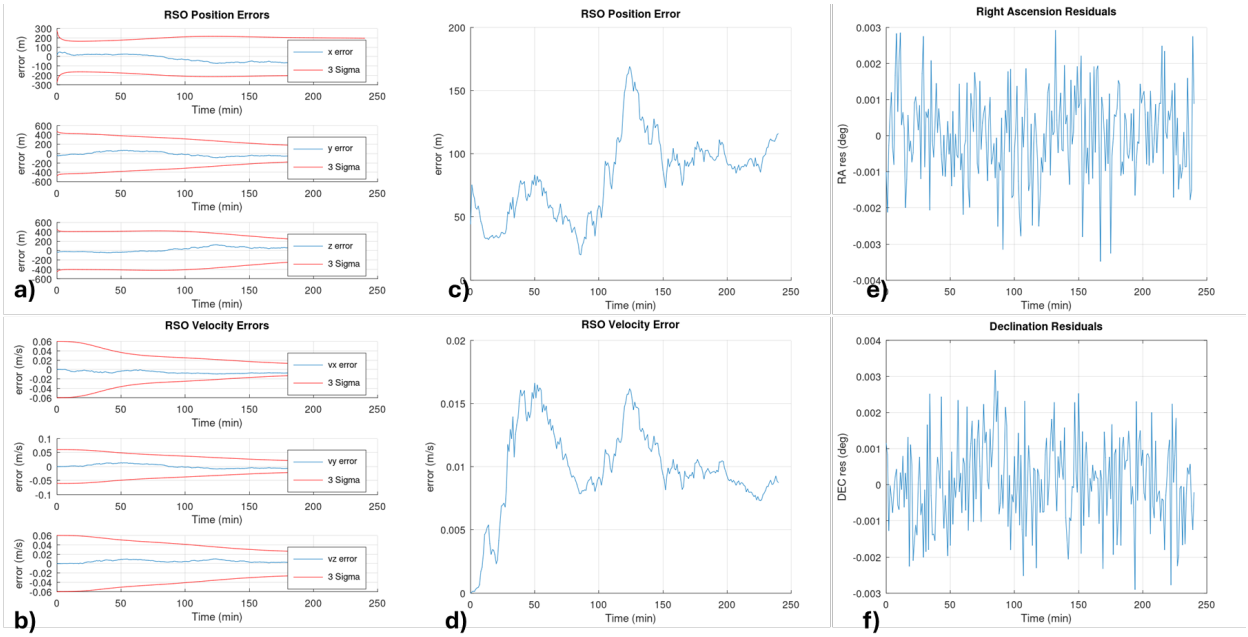

Fig. 14: Errors in position and velocity of Anik F1R as solved by the EKF. Panels a) and b) show the position and velocity errors in each axis, along with the filter's 3-σ covariance bound. Panels c) and d) show the Euclidean norm of the component errors in position and velocity. Panels e) and f) show the measurement residuals.

We see that, during this phase in its orbit, the patrol satellite in the asynchronous corkscrew configuration achieves

Copyright © 2024 Advanced Maui Optical and Space Surveillance Technologies Conference (AMOS) – www.amostech.com

position and velocity errors of less than 200 m and 2 cm/s, respectively, for its characterization of both Anik F1 and Anik F1R. The measurement residuals hover between +/- 10 arc seconds and look to be fairly Gaussian in their distribution. We summarize the component and Euclidean norm mean errors for the lateral, vertical, and asynchronous corkscrew cases in Table 9 for the 4-hour simulation case, with the best performing patrol orbit types, in terms of minimum normalized position and velocity errors, highlighted in bold font.

Table 9: Summary of mean errors in position and velocity of the Anik satellites for the 4-hour simulation.

Orbit Type	Component	Anik F1		Anik F1R	
		Position Mean Error (m)	Velocity Mean Error (mm/s)	Position Mean Error (m)	Velocity Mean Error (mm/s)
Lateral	X	70.53	4.15	-30.02	-4.58
	Y	8.21	5.29	-18.20	3.39
	Z	8.06	2.47	-10.91	-2.42
	Norm	85.59	8.42	65.03	11.00
Vertical	X	25.69	0.94	-10.05	-5.11
	Y	-3.98	2.14	5.68	5.02
	Z	1.80	2.52	-23.99	-3.82
	Norm	**35.43**	**5.09**	**53.37**	11.23
Corkscrew	X	53.82	0.85	-30.86	-5.89
	Y	15.93	5.38	-21.93	-0.95
	Z	-33.45	2.31	28.30	3.81
	Norm	70.65	6.42	81.73	**9.90**

The 24-hour simulations (with gaps in observations due to detection constraints) are summarized with plots showing the errors in position and velocity estimates as calculated by the EKF from each patrol orbit type to both Anik satellites in Figure 15. We include the errors as calculated by the UKF for the ground-based observer to serve as a baseline for comparison to the space-based results. We see that the patrol orbits are able to estimate the position and velocity of the Anik satellites with smaller errors ($\sim$ sub kilometer in position, sub 10 cm/s in velocity) in comparison to the ground-based observer. We also note that the observation blackout period is much larger for the ground-based observer, as it loses signal midway through the simulation (due to daylight constraints), while the satellites in patrol orbits experience signal outages, but recover visibility to the RSO more quickly.

Copyright © 2024 Advanced Maui Optical and Space Surveillance Technologies Conference (AMOS) – www.amostech.com

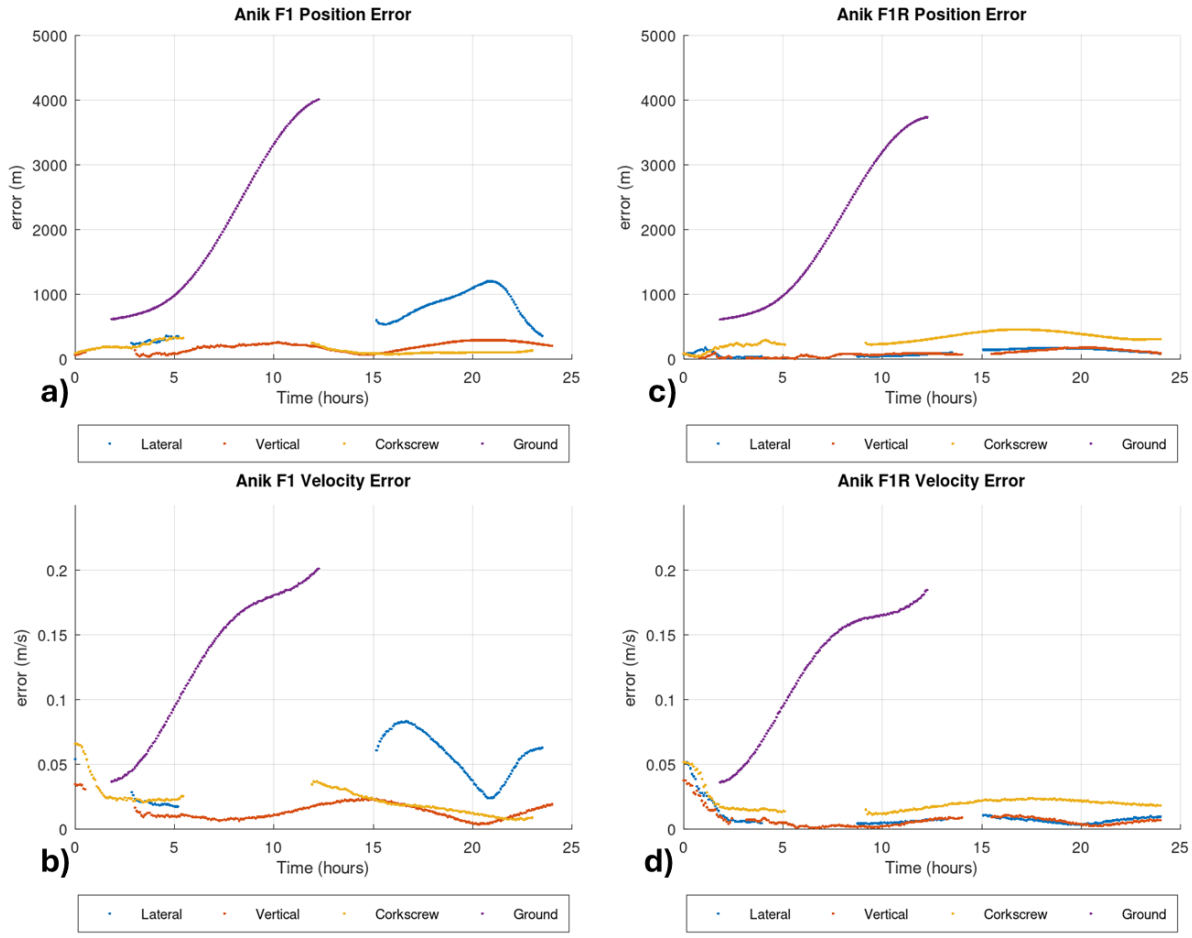

Fig. 15: Errors in position and velocity estimates of the Anik F1 and F1R satellites over 24-hours as generated by the various satellites in patrol orbits and by the ground.

In both simulations, the vertical patrol orbits provide the lowest errors in position and velocity errors, understandably, as the orbit is closest to the Anik satellites, and thus provides the most detection opportunities. We plot the 3-σ error ellipsoids of Anik F1 and Anik F1R in relation to each other as determined at the end of the 24-hour simulation by the satellite in the vertical patrol orbit. Because of the small covariances found, we needed to increase the scale of the error ellipsoids by 1000 times to be visible. These results demonstrate the utility of nearby patrol orbits for on-orbit characterization of objects through optical observation. The asynchronous corkscrew orbit goes a step further, and enables monitoring of the full GEO belt of satellites with the ability to conduct orbit determination analyses during the limited time it has available when within view of an RSO of interest.

Copyright © 2024 Advanced Maui Optical and Space Surveillance Technologies Conference (AMOS) – www.amostech.com

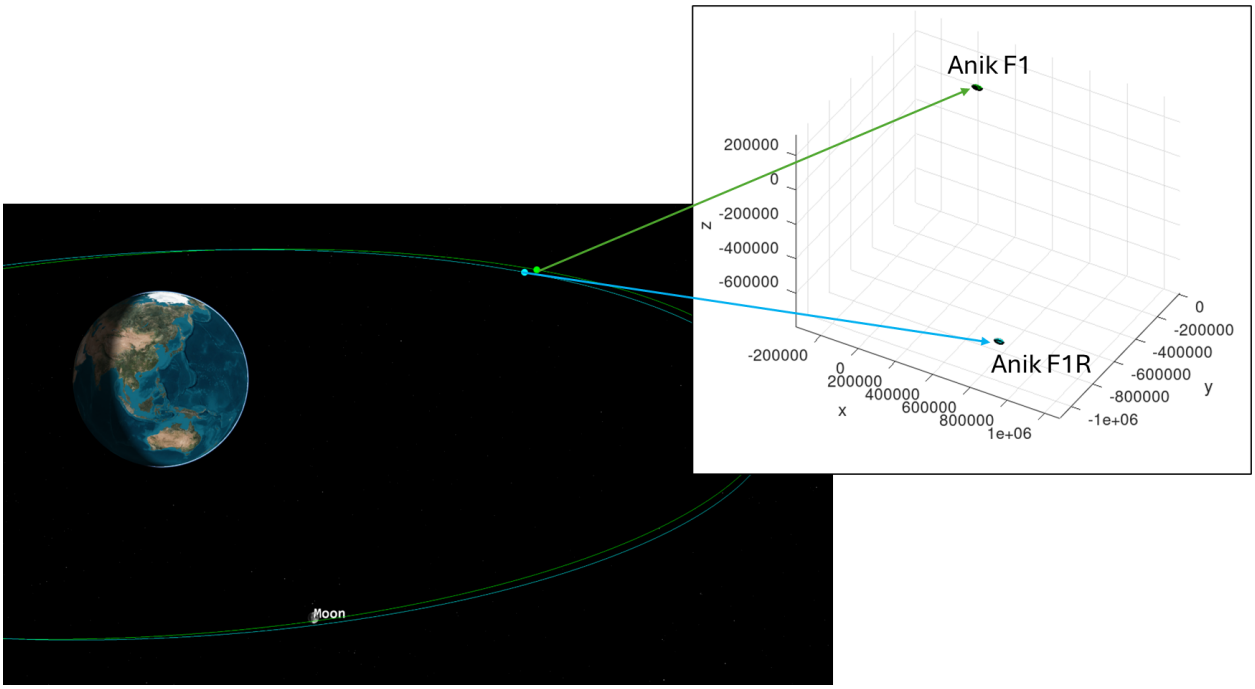

Fig. 16: The Anik F1 and F1R 3σ error ellipsoids (increased in scale by 1000), as determined by the satellite in the vertical patrol orbit after one day of observations (filtered by the ability to detect).

4. SUMMARY AND CONCLUSIONS

An investigation of the various patrol orbits and their utility for surveillance of a specific region of the geostationary belt was conducted. We described the fundamental characteristics of patrol orbits and presented a differentiated patrol orbit type, called the asynchronous corkscrew orbit, that allows a satellite to tour the full circumference of GEO through a longitudinal drift parameter. We conducted a trade study of patrol orbit parameters to find a set for each patrol orbit type that optimized detections of the Anik F1 and F1R satellites. Using the optimized patrol orbits, we assessed and compared position and velocity errors of the Anik satellites as perceived from optical payloads on the patrol satellites and using a two-body OD filter. We demonstrated that, given good initialization of the filter, the patrol orbits can readily distinguish between the states of the Anik F1 and F1R satellites, as their position error covariance ellipsoids are discernably separated.

5. FUTURE WORK

In future iterations of this work, the authors recommend further investigation into the optimization of on-board orbit determination algorithms. Fusion of measurements from multiple patrol satellites and supplemental measurements from ground sites in a single filter could improve detectability and reduce uncertainty. Exploration of filter tuning, addition of process noise, including other unmodeled dynamics, or use of entirely different orbit determination filters, including the UKF or Particle Filters, could serve to improve filter performance.

Another topic rich with potential is further characterization and exploration of the use of asynchronous corkscrew patrol orbits for deterrence activities for objects throughout the GEO belt. Because of their dynamic nature, a constellation of satellites in this type of patrol orbit could provide continuous surveillance of the belt. One could investigate the size and orbit characteristics of such a constellation, develop payload and satellite specifications for monitoring activities, or future mature the CONOPs for a potential mission.

Copyright © 2024 Advanced Maui Optical and Space Surveillance Technologies Conference (AMOS) – www.amostech.com

Disclaimer

The views expressed in this paper are those of the authors and do not reflect the official policy or position of the United States Air Force, United States Space Force, Department of Defense, or the U.S. Government.

References

[1] B. Thompson, T. Kelecy, T. Kubancik, T. Flora, M. Chylla and D. Rose, "Geosynchronous patrol orbit for space situational awareness," in Advanced Maui Optical and Space Surveillance Technologies Conference (AMOS), Maui, HI, 2017. https://amostech.com/TechnicalPapers/2017/Poster/Kelecy.pdf

[2] S. Erwin, "Space Force: We expect to see 'interfering, blinding' of satellites during conflict," 15 March 2023. [Online]. Available: https://spacenews.com/space-force-we-expect-to-see-interfering-blinding-of-satellites-during-conflict/.

[3] M. Schierholtz, T. Kubancik, K. Charles, I. Hussein, E. Griggs, B. Thompson and E. Silva, "Geosynchronous Patrol Orbits for Optimized GEO Space Domain Awareness," in Advanced Maui Optical and Space Surveillance Conference (AMOS), Maui, HI, 2023. https://amostech.com/TechnicalPapers/2023/Poster/Schierholtz.pdf

[4] K. Simon, "Passive RF in Support of Closely Spaced Objects Scenarios," in Advanced Maui Optical and Space Surveillance Technologies Conference (AMOS) , Maui, HI, 2020. https://amostech.com/TechnicalPapers/2020/Astrodynamics/Simon.pdf

[5] K. A. Sebastian, "UCS Satellite Database," 1 May 2023. [Online]. Available: https://www.ucsusa.org/resources/satellite-database#.W7WcwpMza9Y.

[6] T. Kelecy, S. Abernethy, F. Jones, E. Gerber and H. Wurzel, "Predicted Intent Inferred from Real-time Rendezvous and Proximity Behavior," in Advanced Maui Optical and Space Surveillance Technologies Conference (AMOS), Maui, HI, 2022. https://amostech.com/TechnicalPapers/2022/Conjunction-RPO/Kelecy.pdf

[7] J. Tompkins, S. Cain and D. Becker, "Near earth space object detection using parallax as multi-hypothesis test criterion," *Optics Express*, Vol. 27, No. 4, Feb. 18 2019. https://opg.optica.org/oe/fulltext.cfm?uri=oe-27-4-5403&id=405059

[8] R. Scott and B. Wallace, "Small Aperture Telescope Observations of Co-located Geostationary Satellites," in Advanced Maui Optical and Space Surveillance Technologies Conference (AMOS), Maui, HI, 2009. https://amostech.com/TechnicalPapers/2009/Poster/Scott.pdf

[9] J. Tombasco, "Orbit Estimation of Geosynchronous Objects Via Ground-Based and Space-Based Optical Tracking," PhD dissertation, University of Colorado, 2011. https://scholar.colorado.edu/concern/graduate_thesis_or_dissertations/9593tv387

[10] E. Fehlberg, "Classical Fifth-, Sixth-, Seventh-, and Eighth-Order Runge-Kutta Formulas with Stepsize Control," NASA TR R-287, NASA George C. Marshall Spaceflight Center, Huntsville, Alabama, 1968. https://ntrs.nasa.gov/api/citations/19680027281/downloads/19680027281.pdf

[11] S. Pines, "Uniform Representation of the Gravitational Potential and its Derivatives," *AIAA Journal*, Vol. 11, No. 11, 1973.

[12] General Dynamics, "Sentinel M-Code GPS Receiver," 2023. [Online]. Available: https://gdmissionsystems.com/-/media/general-dynamics/space-and-intelligence-systems/pdf/space-sentinel-m-code-gps-receiver-datasheet.ashx

[13] Airbus Defence and Space, "Space Equipment Avionics – GEO MosaicGNSS Receiver," 2018. [Online]. Available: https://satcatalog.s3.amazonaws.com/components/30/SatCatalog_-_Airbus_-_GEO_MoasaicGNSS_Receiver_-_Datasheet.pdf?lastmod=20210708014811

[14] D.A. Vallado, *Fundamentals of Astrodynamics with Applications*, 5th ed., Microcosm Press, Hawthorne, California, 2022.

Copyright © 2024 Advanced Maui Optical and Space Surveillance Technologies Conference (AMOS) – www.amostech.com